Available online at www.sciencedirect.com
ScienceDirect
Inorganica Chimica Acta 361 (2008) 956–964
Inorganica Chimica Acta
www.elsevier.com/locate/ica

When identical functional groups are not identical: A DFT study of the effects of molecular environment on sulfur K-edge X-ray absorption spectra

Ritimukta Sarangi [a], Patrick Frank [a,b], Keith O. Hodgson [a,b,*], Britt Hedman [b,*]

[a] Department of Chemistry, Stanford University, Stanford, CA 94305, USA
[b] Stanford Synchrotron Radiation Laboratory, SLAC, Stanford University, Stanford, CA 94309, USA

Received 24 April 2007; accepted 15 May 2007
Available online 5 June 2007

Dedicated to Edward I. Solomon

Abstract

Density functional theory (DFT) and time-dependent DFT (TD-DFT) calculations have been used to elucidate differences in the sulfur K-edge spectra of three pairs of related compounds: methionine and $S(Me)_3^+$, cystine and (±)6-thioctic amide, and $(Me)_2SO_3$ and $(CH_2)_2SO_3$. TD-DFT is shown to accurately reproduce all the experimental XAS spectra. The 2 eV energy difference in the sulfur K-edge rising edge position between methionine and trimethylsulfonium is shown to derive from changes in bonding rather than the increase in effective nuclear charge. A similar insensitivity to effective nuclear charge is found in the XAS spectra of cystine and (±)6-thioctic amide. These surprising results are traced back to the fact that XAS spectra reflect orbital energy differences, rather than a measure of the atomic potential. The change in atomic potential following oxidation or reduction affects the core and valence orbitals almost equally. In all cases DFT calculations showed that the dramatic differences in sulfur K-edge spectra found between functional groups in alternative molecular environments derive from the variations in orbital mixing and energies following from bonding. However, XAS rising-edge energy positions have a near linear correlation with oxidation state. This is attributed to the fact that bond strength typically increases with oxidation state. Therefore, although XAS rising-edge energies are an approximate measure of the oxidation state of the absorbing atom, it is important to recognize that the correlation of XAS edge energy with effective nuclear charge is not direct. This result is finally applied to the question of quantitative sulfur speciation in complex materials of chemical, biological, or geological origin.

Keywords: S K-edge; XAS; DFT; Bonding

1. Introduction

Ever since the foundational papers of George and Gorbaty [1], George et al. [2] and Waldo et al. [3] sulfur K-edge X-ray absorption spectroscopy (XAS) has been used to quantify sulfur within a variety of complex materials [4,5]. In this method, the sulfur K-edge spectrum of a sample that includes a complex mixture of sulfur-containing molecules can be reproduced in terms of a linear combination of the sulfur K-edge spectra of known model compounds. In this way, a quantitative estimate of all the major sulfur-containing functional groups in the original sample may be obtained.

However, since then a view has evolved assuming that fits to the sulfur K-edge spectra of complex materials might proceed on the assumption that the XAS spectrum of any given sulfur functional group is, for practical purposes, nearly invariant with local chemical structure [6–12]. Thus, the sulfur K-edge XAS spectrum of cystine, for example,

* Corresponding authors. Address: Stanford Synchrotron Radiation Laboratory, SLAC, Stanford University, Stanford, CA 94309, USA. Tel.: +1 650 926 3052; fax: +1 650 926 4100.
E-mail addresses: hodgson@ssrl.slac.stanford.edu (K.O. Hodgson), hedman@ssrl.slac.stanford.edu (B. Hedman).

0020-1693/$ - see front matter © 2007 Elsevier B.V. All rights reserved.
doi:10.1016/j.ica.2007.05.047

might be used to quantify the level of unknown disulfides in a variety of milieus. It has been known for some time that the sulfur K-edge spectra of molecules as different as cysteine and sulfate are sensitive to the degree of protonation [13–15]. More recently, it was explicitly shown that relatively minor variations in the local molecular bonding environment could produce very different sulfur K-edge spectra for otherwise identical sulfur functional groups [16]. In addition, the XAS spectra of some sulfur compounds can include features at energies otherwise consistent with more highly oxidized sulfur, which can lead to spurious qualitative assignments.

In purely ionic compounds, sulfur K-edge transitions are associated with the 1s→4p and 1s→continuum transitions. However, sulfur, in a wide range of oxidation states (−2 to +6), forms strong covalent bonds in both organic and inorganic molecules. In these cases the transitions also include 1s→φ^*, where φ^* represents all unoccupied molecular orbitals (MOs) with significant contribution from a sulfur atomic orbital with *p*-symmetry. The composition and relative energy positions of these MOs lead to the signature sulfur K-edge spectrum of a particular functional group. It is generally accepted that the 1s→φ^* transition increases in energy as the oxidation state increases due to change in the effective nuclear charge on the sulfur [17,18]. Thus, the intense rising edge main peak in the sulfur K-edge of inorganic SO_4^{2-} occurs at ~2482.4 eV, ~9 eV higher than that of S_8 (~2472.8 eV).

In this study, DFT calculations are used to define the bonding and valence level orbitals of three groups of sulfur-containing molecules that embody identical structural groups modified by distinct molecular environments. Time-dependent DFT (TD-DFT) calculations are then used to test the derived orbital assignments against the sulfur K-edge XAS spectra of these molecules. The effects of charge and of bonding on sulfur K-edge spectra are evaluated separately. Finally, the differences observed in the sulfur K-edge spectra are correlated with the bonding within otherwise identical functional groups made unique by their molecular environment.

2. Experimental

2.1. Sample preparation

Unless otherwise noted, all compounds were used as received from Aldrich Chemical Company. L-Methionine (**1a**) was prepared as a 50 mM solution in 250 mM citrate, pH 7.1. Trimethylsulfonium iodide (**1b**) was prepared as a 0.1 M solution in deionized water. Ethylene cyclic sulfite (**2a**) and dimethyl sulfite (**2b**) were prepared as 0.1 M solutions in *p*-xylene. Dimethyl sulfite was pre-purified by fractional distillation from anhydrous sodium carbonate. Cystine (**3a**) was prepared as a saturated (<0.1 M) solution in 250 mM aqueous citrate, pH 7.1. (±)6-Thioctic amide (**3b**) was ground using an agate mortar and pestle and prepared as powder on sulfur-free tape.

2.2. Sulfur K-edge data

Sulfur K-edge spectra of **1a**, **1b**, **2a**, **2b**, **3a**, and **3b** were measured using the SSRL 54-pole wiggler beam line 6-2 in high magnetic field mode of 10 kG with a Ni-coated harmonic rejection mirror and a fully tuned Si(1 1 1) double crystal monochromator. Details of the optimization of this beam line for low energy fluorescence measurements and the experimental setup have been described previously [19,20]. External energy calibration and data normalization were performed as described in earlier publications [21]. The area under the pre-edge peak was quantified by fitting the data using EDG_FIT [22]. The pre-edge and rising edge features were modeled with pseudo-Voigt line-shapes with a fixed 1:1 Lorentzian:Gaussian ratio. Normalization procedures introduce ~3% error in the value of the integrated area under the pre-edge peak.

2.3. Electronic structure calculations

Gradient-corrected, (GGA) restricted density functional calculations were carried out using the GAUSSIAN03 package [23] on a 2-CPU Linux-based computer. Geometry optimizations were performed for each complex. The BECKE88 [24,25] exchange and PERDEW86 [26,27] correlation nonlocal functionals with Vosko–Wilk–Nusair [28] local functionals as implemented in the software package (BP86) were employed in this study to compare the electronic structure differences in **1a**, **1b**, **2a**, **2b**, **3a**, and **3b**. The double-ζ 6-31G* basis set [29–31] was used for all atoms. Population analyses were performed by means of Weinhold's Natural Population Analysis (NPA) [32–34]. Wave functions were visualized and orbital contour plots were generated in Molden [35]. Compositions of molecular orbitals and overlap populations between molecular fragments were calculated using the PYMOLYZE program [36].

2.4. TD-DFT calculations

TD-DFT calculations were performed with the electronic structure program ORCA [37,38]. Single point ground state DFT calculations with the BP86 functional were performed using the geometry optimized coordinates obtained from GAUSSIAN03. The double-ζ 6-31G* basis set was used for all atoms. The symmetry equivalent S 1s orbitals were localized, and only excitations from the localized S 1s orbitals to the lowest unoccupied orbitals were allowed.

3. Results and analysis

3.1. Comparison of $S(Me)_2$ (*1a*) and $[S(Me)_3]^+$ (*1b*)

3.1.1. Sulfur K-edge

Fig. 1 shows structural diagrams of all the sulfur functional groups in the study reported here. These structures were used for the DFT and TD-DFT calculations, and

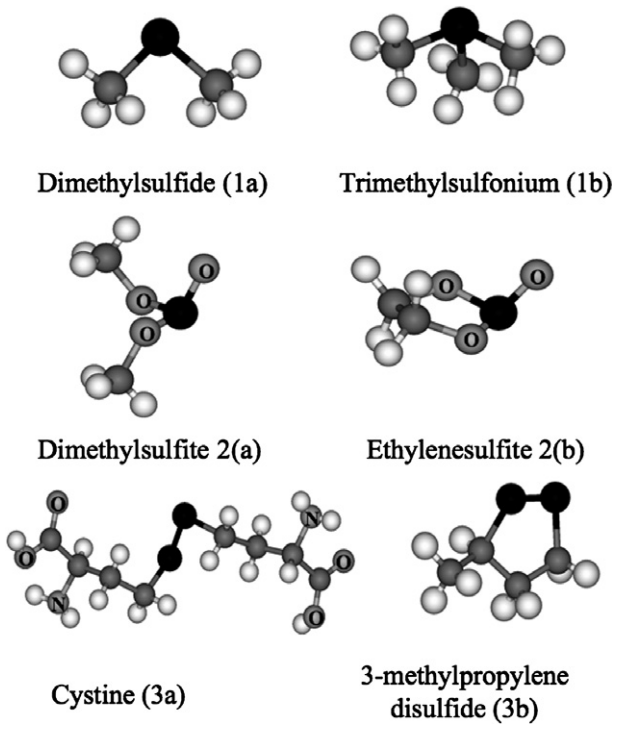

Fig. 1. Structures of the modified versions of **1a**, **1b**, **2a**, **2b**, **3a** and **3b** as used for DFT and TD-DFT calculations. Unlabelled S, C and H atoms are shown as black, gray and light-gray spheres, respectively.

either represent, or were adapted from $(S(Me)_2$, 3-methylpropylenedisulfide, dimethylsulfite, ethylenesulfite), known molecular structures [39–45].

A comparison of the sulfur K-edge XAS spectra and the second derivative spectra of **1a** and **1b** are shown in Fig. 2 and (inset), respectively. It should be noted that the sulfur K-edge XAS spectrum of L-methionine was chosen to represent $S(Me_2)$ (**1a**). DFT calculations performed on L-methionine showed that the bonding and valence level energy splittings in $S(Me)_2$ are very similar to those in methionine (see Figure S1, Supplementary material). Sulfur

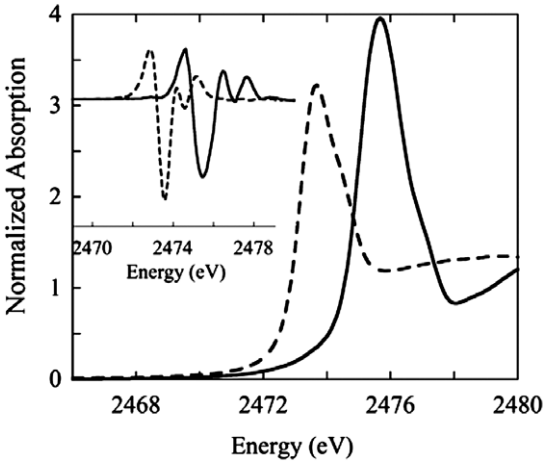

Fig. 2. The sulfur K-edge XAS spectra of **1a** (----) and **1b** (—). The inset shows the second derivative spectra.

K-edge XAS transitions are localized on the absorbing atom and are dipole-allowed but quadrupole-forbidden. Thus, only the transitions corresponding to S 1s→np will have intensity in sulfur K-edge spectra [46]. In **1a**, an intense low energy transition is observed at 2473.6 eV followed by a less intense higher energy shoulder at 2474.6 eV. These two features are followed by several relatively weak transitions that overlap with the S 1s→4p transition and together constitute the post-edge region. The sulfur K-edge spectrum of **1b** is shifted to higher energy relative to **1a** by 1.9 eV. Similar to **1a**, a low energy intense transition is observed at 2475.5 eV followed by a less intense shoulder at 2477.0 eV. Since sulfur K-edge XAS transitions are electric dipole-allowed and localized on the S atom, the transition intensity for any S 1s→φ^* transition, where φ^* is any valence level MO, directly reflects the amount of sulfur np character mixed into φ^*. Thus, the high intensity of the two low-lying transitions in both **1a** and **1b** reflect transitions to predominantly sulfur-based 3p orbitals.

3.1.2. DFT calculations

To shed light on the role of the nature of bonding in **1a** and **1b**, spin-restricted DFT calculations were performed. The oxidative addition of a methyl group to $S(Me)_2$, producing $S(Me)_3^+$, leads to an increase in the charge on the sulfur atom (Q^S_{mol}) and an increase in bonding interaction due to the presence of an additional methyl group, which converts the planar $S(Me)_2$ to the pyramidal $S(Me)_3^+$. Both these factors affect the energy levels of **1a** relative to **1b** and hence the sulfur K-edge energy position.

In order to understand the dominant contribution to the shift in the edge energy positions, a third calculation was performed on the radical cation $[S(Me)_2]^{+\cdot}$ (**1c**). This species has the same ligand set as $S(Me)_2$ but a sulfur atom with the similar net charge as in $S(Me)_3^+$. The Mulliken charges and lowest energy sulfur K-edge transitions for **1a**, **1b** and **1c** (represented as $\Delta E(\varphi^*_{LUMO}\text{-}1s)$) are shown in Table 1. Fig. 3 compares the core and valence energy level of **1a**, **1b** and $[S(Me)]_2^{+\cdot}$ obtained from DFT calculations. The $\Delta E(\varphi^*_{LUMO}\text{-}1s)$ for **1a** and **1b** differ by 2 eV, which is in good agreement with the 1.9 eV shift derived experimentally. A comparison shows that the Mulliken charge increases in the order **1a** < **1b** < $[S(Me)_2]^{+\cdot}$. However, the $\Delta E(\varphi^*_{LUMO}\text{-}1s)$ is lowest for $[S(Me)_2]^{+\cdot}$. In $S(Me)_2$ the S $3p_x$ and $3p_y$ orbitals have an in-plane bonding interaction with the –Me group. The $3p_x$ is spatially oriented to have a more favorable interaction with the C 2p orbitals of both the –Me groups relative to the S $3p_y$

Table 1
Selected DFT parameters

	Mulliken charge S (C)	$\Delta E(\varphi^*_{LUMO}\text{-}1s)$ (eV)
1a	0.095 (−0.61)	2398.0
1b	0.56 (−0.65)	2400.0
$[S(Me)_2]^{+\cdot}$	0.65 (−0.71)	2394.6

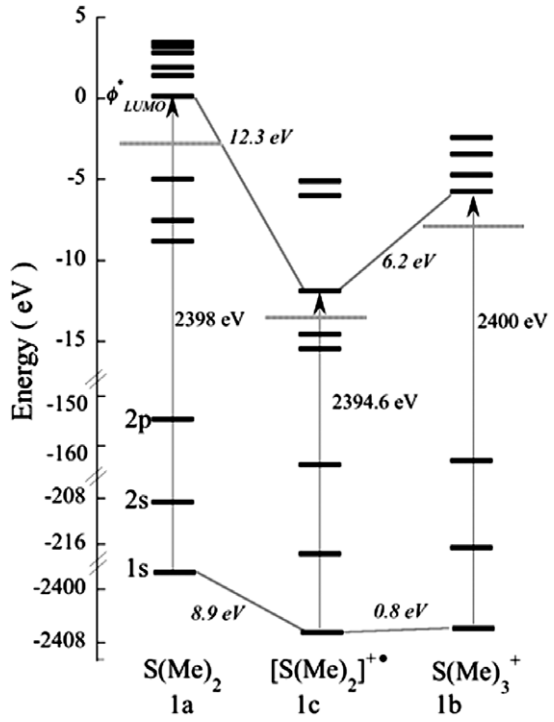

Fig. 3. DFT calculated core and valence level energies. The gray horizontal dashed line in each ladder marks the $\varphi^*_{HOMO} - \varphi^*_{LUMO}$ energy divide. The relative spacing in core level energies (1s, 2s, 2p) remains similar in $S(Me)_2$, in $[S(Me)_2]^{+\cdot}$ after oxidation by a single electron, and in $S(Me)_3^+$ following the oxidative addition of a methyl group. However, the valence level energies are disparate due to changes in bonding, producing the difference in $\Delta E(\varphi^*_{LUMO}\text{-}1s)$ (represented by arrows). Note that the φ^*_{HOMO} in $S(Me)_2$ becomes the φ^*_{LUMO} in $[S(Me)_2]^{+\cdot}$ and XAS $\Delta E_{\varphi^*_{LUMO}\text{-}1s}$ is larger in $S(Me)_2$ than in $[S(Me)_2]^{+\cdot}$, so that oxidation would produce a new sulfur K-edge XAS spectrum at *lower* energy.

orbitals. Hence the φ^*_{LUMO} and φ^*_{LUMO+1} (which involve the anti-bonding combination of S $3p_x$ and $3p_y$ with C 2p, respectively) are split by ~1.5 eV (consistent with the experimentally observed transition energies (see Section 3.1.1)). The $3p_z$ orbital is out-of-plane and remains non-bonding.

In $S(Me)_2^{+\cdot}$, this $3p_z$ orbital, (which is the φ_{HOMO} in $S(Me)_2$) gets depopulated (oxidation of $S(Me)_2$ to $S(Me)_2^{+\cdot}$) and becomes the new φ^*_{LUMO}. The loss of this electron and the resulting positive charge lower the energy of the new $3p_z$ φ^*_{LUMO}, relative to the original filled non-bonding $3p_z$ orbital. However, the lowered energy of the $3p_z$ orbital is not fully compensated by the lower energy of the S1s orbital, thus the transition energy, $\Delta E(\varphi^*_{LUMO}\text{-}1s)$, decreases on oxidation. In $S(Me)_3^+$, the situation is very different. The pyramidal geometry allows strong interaction of the $3p_z$ of sulfur with the –Me group, which results in significant sulfur $3p_x$, $3p_y$ and $3p_z$ contributions to φ^*_{LUMO}, φ^*_{LUMO+1} and φ^*_{LUMO+2}, respectively. The pyramidal geometry leads to similar overlap of the sulfur $3p_x$ and $3p_y$ with the carbon 2p of the –Me groups. The result is a near degeneracy in the φ^*_{LUMO} and φ^*_{LUMO+1} orbital energy levels $[\Delta E(\varphi^*_{LUMO+1} - \varphi^*_{LUMO}) = 0.008\ eV]$. In addition the φ^*_{LUMO} is destabilized in $S(Me)_3^+$ relative to that in $S(Me)_2$. This can be clearly seen in Fig. 3, which shows that all the core and bonding level orbitals are shifted by approximately the same energy indicating that an increase in charge on sulfur in $S(Me)_3^+$ affects all orbitals equally. However, due to differences in bonding (*vide infra*), the φ^*_{LUMO} in $S(Me)_3^+$ is destabilized relative to that in $S(Me)_2$ and hence the transition energy $\Delta E(\varphi^*_{LUMO}\text{-}1s)$ is higher.

The point to note here is that the increase in charge did not shift the rising edge energy of $S(Me)_3^+$ 2 eV relative to that of $S(Me)_2$. Comparison of $S(Me)_2$ with $S(Me)_2^{+\cdot}$ in Fig. 3 shows that oxidation is predicted to *lower* the sulfur K-edge φ^*_{LUMO}-1s energy by 3.4 eV. This result contradicts the usual argument made in terms of oxidation state [3,16,47–49]. Rather, the source of the relative energy shift of the sulfur K-edge XAS energies that distinguishes $S(Me)_3^+$ from $S(Me)_2$ is the change in bonding. If the bonding effects did not shift the φ^*_{LUMO} to higher energy, the increase in charge on going from $S(Me)_2$ to $S(Me)_3^+$ would lower the energy of both the valence orbital and the 1s orbital similarly. The *relative* energy between S φ^*_{LUMO} and S 1s would thus not be perturbed significantly and there would be little or no observable shift in rising K-edge energies. Thus the comparison of the Mulliken charge and calculated edge energy shifts in $S(Me)_2$, $S(Me)_2^{+\cdot}$ and $S(Me)_3^+$ demonstrates that the charge on the S atom has a relatively minor effect in determining the sulfur K-edge energy position. The major observed effect stems from bonding.

3.2. Comparison of $(CH_2)_2SO_3$ (**2a**) and $(Me_2)SO_3$ (**2b**)

3.2.1. Sulfur K-edge

A comparison of the sulfur K-edge XAS spectra and the second derivative spectra of **2a** and **2b** are shown in Fig. 4a and (inset), respectively. In **2a**, three transitions are observed between 2476 and 2480 eV, at 2476.9 eV, 2478.7 eV and 2479.8 eV, which can be associated with low-lying valence orbitals. The sulfur K-edge spectrum of **2b** also has three low-lying transitions, however, the intensity and energy position of these transitions are significantly different from those of **2a**. The lowest energy transition occurs at 2477.3 eV, ~0.4 eV higher than that in **2a**. The second peak occurs at 2478.2 eV indicating an energy split of ~0.9 eV relative to the 1.8 eV energy split between the two lowest energy peaks of **2a**. The third peak occurs at 2479.7 eV and is similar in energy and intensity to that observed for **2a**.

3.2.2. DFT calculations

Spin-restricted DFT calculations were performed on **2a** and **2b**. Relevant structural parameters are listed in Table 2. The bond distance parameters are very similar in the two complexes. However, the two constrained CH_2-groups in **2a** optimize to a cis-conformation while the free methyl groups in **2b** optimize to the trans-form, which leads to a

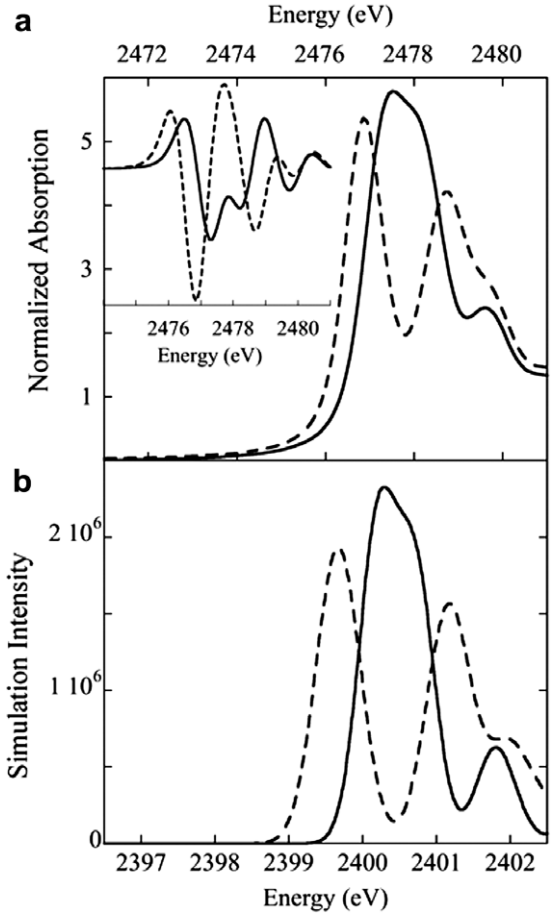

Fig. 4. (a) S K-edge XAS spectra of **2a** (----) and **2b** (—). Inset shows the second derivative spectra. (b) The TD-DFT calculated S K-edge spectra of **2a** (----) and **2b** (—). The transitions have been convolved with a pseudo-Voigt function of 0.5 eV half-width to account for experimental and core-hole broadening.

wider ∠OSO (119° in **2b** relative to 91° in **2a**). This also leads to shorter S–O bonds in **2b** relative to those in **2a** (Table 2). In both **2a** and **2b**, the φ^*_{LUMO}, φ^*_{LUMO+1} and φ^*_{LUMO+2} have dominant S 3p character and lead to the three low-lying transitions observed in their respective sulfur K-edge spectra. The shorter S–O bond distance in **2b** allows for a stronger interaction of the S $3p_x$ and O 2p orbitals leading to a destabilized φ^*_{LUMO} in **2b** relative to that in **2a**. However, the smaller angle ∠OSO in **2a** allows for a better overlap of the S $3p_y$ and O 2p orbitals relative to that in **2b** and hence destabilizes the φ^*_{LUMO+1}. This is reflected in the large increase in the O 2p character in φ^*_{LUMO+1} in **2a** relative to **2b** (Table 2). The S═O bond (S $3p_z$ and O 2p σ overlap) is relatively unaffected by the structural change between **2a** and **2b** and hence, the energies of the φ^*_{LUMO+2} orbitals are similar.

To further support the DFT calculated energy levels, TD-DFT calculations were performed for the S 1s→continuum transitions. The TD-DFT calculations reproduce the sulfur K-edge transition energy and intensity and give clear evidence that the structural change modifies the orbital overlap, which in turn governs the sulfur K-edge XAS spectra. The simulated spectra are shown in Fig. 4b and a correlation of the orbital energies, orbital contour plots and the sulfur K-edge data are shown in Fig. 5. In **2a** the $1s \rightarrow \varphi^*_{LUMO}$ transition is lower in energy than that in **2b** by 0.4 eV. However, the $1s \rightarrow \varphi^*_{LUMO+1}$ is *higher* in energy by 0.5 eV in **2a**. If the shifts in the edge transition energy were associated solely with charge, the energy positions for all transitions would uniformly shift to higher energy with an increase in charge. Thus, the relative trend in the edge energies of **2a** and **2b** gives further evidence that shifts in rising-edge energies are predominantly due to differences in bonding.

Table 2
Selected DFT parameters

	Bond distance (Å)			Mulliken charge				Mulliken spin density (%)				
	S═O	S–O	O–C[a]	S	O(O^D)[b]	C		S(p)	O^D	O1[c]	O2[d]	C,H
2a	1.48	1.72	1.45	0.964	−0.470 (−0.52)	0.25	φ^*_{LUMO}	63.1	17.8	4.8	5.0	9.7
							φ^*_{LUMO+1}	62.0	9.8	13.4	12.6	9.7
							φ^*_{LUMO+2}	64.1	11.8	5.0	4.9	20.9
2b	1.48	1.70	1.45	0.984	−0.5 (−0.5)	0.26	φ^*_{LUMO}	63.6	14.2	5.8	9.2	9.2
							φ^*_{LUMO+1}	64.4	9.7	9.7	9.1	10.3
							φ^*_{LUMO+2}	61.6	14.5	2.1	6.6	20.3
	S–S	S_1–C_1[e]	S_2– C_2[e]	S_1	S_2	$C_1(C_2)$		S_1(p)	S_2(p)	C	S(s)	N,C,H,O
3a	2.10	1.86	1.86	0.012	0.012	−0.47 (−0.47)	φ^*_{LUMO}	46.0	46.0	3.6	1.0	4.0
							φ^*_{LUMO+3}	22.3	22.3	26.3	3.8	26.2
							φ^*_{LUMO+4}	24.0	24.1	26.8	6.4	18.6
3b	2.11	1.87	1.86	0.016	0.024	−0.46 (−0.29)	φ^*_{LUMO}	47.8	45.0	3.7	1.0	3.0
							φ^*_{LUMO+1}	20.0	29.0	36.8	5.4	9.2
							φ^*_{LUMO+2}	32.2	21.9	29.6	1.7	14.1

[a] The two C–O and S–O (single-bond) distances differ by >0.01 Å in **2a** and **2b**. The values listed here are the average bond distances.
[b] O^D refers to the S═O oxygen.
[c] O1 refers to the O atom which is connected to the methyl group cis to the S═O (see contour plot, Fig. 5).
[d] O2 refers to the O atom which is connected to the methyl group trans to the S═O (see contour plot, Fig. 5).
[e] The two S–C bond distances are given separately to emphasize the asymmetry in **3b**.

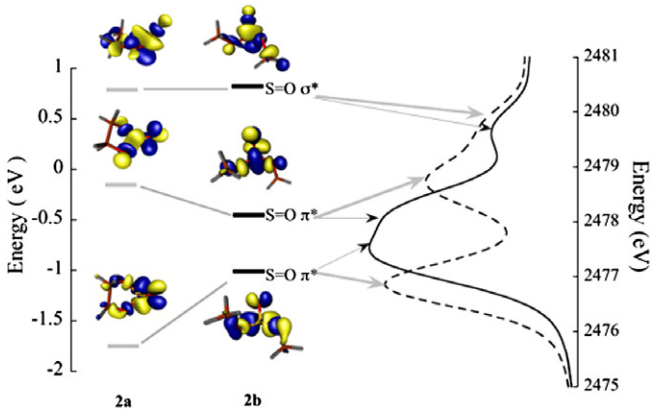

Fig. 5. (Left panel) The DFT calculated valence energy level and the corresponding contour plots. (Right panel) The energy levels are correlated to the S K-edge transitions. The gray and black arrows (pointing to the transition energies) correspond to **2a** and **2b** energy levels, respectively.

3.3. Comparison of cystine (*3a*) and thioctic acid (*3b*)

3.3.1. Sulfur K-edge

A comparison of the sulfur K-edge XAS spectra and the second derivative spectra of **3a** and **3b** are shown in Fig. 6a and (inset), respectively. Since both cystine and thioctic acid have a disulfide bond, the sulfur K-edge XAS spectra are expected to have dominant contributions from transitions from the S 1s orbital to S–C(σ) + S–S(π) and S–S(σ) based valence anti-bonding orbitals. The sulfur K-edge spectrum of **3a** has two intense transitions at 2472.6 eV and 2474.2 eV followed by continuum level transitions starting at ~2478 eV. In contrast, the sulfur K-edge spectrum of **3b** exhibits three low-lying transitions at 2472.1 eV, 2473.8 eV and 2475.4 eV.

3.3.2. DFT calculations

Spin-restricted DFT calculations were performed on **3a** and a simplified model of **3b** (see Fig. 1). Relevant structural parameters, Mulliken charge and population analyses are listed in Table 2. In **3a** (cystine) the two S atoms are symmetric, which is reflected in very similar Mulliken charges and valence orbital compositions. However, in **3b**, one of the sulfur α-carbon atoms has an alkyl side-chain, which makes the two sulfur atoms dissimilar. The S–C bond distance (S_2–C_2) is slightly shorter than S_1–C_1, which is reflected in the different Mulliken charges and sulfur characters in the relevant valence orbitals. A greater charge on S_2 (0.24) is consistent with a smaller contribution to the valence orbitals (~96% over the three orbitals) relative to S_1 (100% over the three orbitals) (see Table 2). Interestingly, although the average charges on the sulfur atoms are higher for **3b** (~0.02) than for **3a** (0.012), the first lowest energy sulfur K-edge transition (Section 3.3.1) occurs at lower energy for **3b** rather than for **3a**. This again indicates that bonding interactions affect the energies of the sulfur K-edge transitions significantly and can mask the effects of charge differences.

Fig. 7 shows a correlation of the calculated DFT energies with the valence orbital contours and the sulfur K-edge

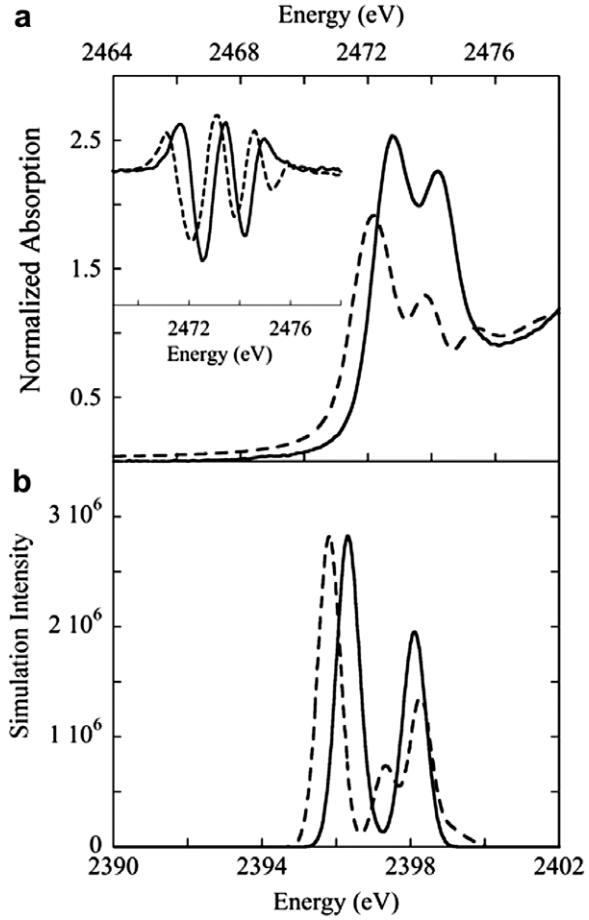

Fig. 6. (a) S K-edge XAS spectra of **3a** (—) and **3b** (----). Inset shows the second derivative spectra. (b) The TD-DFT calculated S K-edge spectra of the model for **3a** (—) and **3b** (----). The transitions have been convolved with a pseudo-Voigt function of 0.5 eV half-width to account for experimental and core-hole broadening.

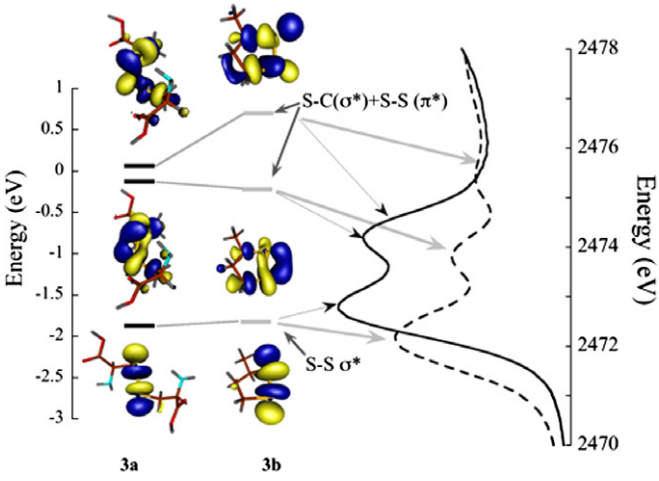

Fig. 7. (Left panel) The DFT calculated valence energy level and the corresponding contour plots. (Right panel) The energy levels are correlated to the S K-edge transitions. The black and gray arrows (pointing to the transition energies) correspond to **3a** and **3b** energy levels, respectively.

XAS spectra of **3a** and **3b**. The φ^*_{LUMO} is dominated by a S–S σ* contribution while φ^*_{LUMO+1} and φ^*_{LUMO+2} include S–S and S–C contributions that are the anti-bonding

combinations of the S–C σ interaction (φ^*_{LUMO+1} and φ^*_{LUMO+2} of **3b** correspond to the φ^*_{LUMO+3} and φ^*_{LUMO+4} in **3a**, respectively, and are referred as such for comparison purposes). In **3a** φ^*_{LUMO+1} and φ^*_{LUMO+2} are very similar in composition (Table 2) and nearly degenerate (Fig. 7) while in **3b** the corresponding two orbitals are different due to the asymmetry in the two sulfur atoms introduced by the presence of the alkyl side-chain. This difference leads to the energy splitting of φ^*_{LUMO+1} and φ^*_{LUMO+2}. The DFT calculated energy difference between φ^*_{LUMO} and φ^*_{LUMO+1} and φ^*_{LUMO+1} and φ^*_{LUMO+2} are 0.8 eV and 0.006 eV in **3a** and 1.6 eV and 0.8 eV in **3b**, which is in reasonable agreement with the sulfur K-edge transition energies. Since a modified version of **3b** was chosen for the DFT calculations, TD-DFT calculations were performed on the DFT models of **3a** and **3b** to test whether the DFT results on the modified version of **3b** are comparable to the sulfur K-edge spectra of **3b**. The results are shown in Fig. 6b. TD-DFT calculations accurately reproduce the energy shift in the three transitions between **3a** and **3b**. However, the intensity calculated pattern of the transitions at 2473.8 eV and 2475.4 eV is different from the experimental intensity pattern. This could indicate a small difference in the model used for DFT and the structure of **3b**. However, the overall agreement between sulfur K-edge data and the simulations are good. Fig. 7 shows that DFT successfully reproduced the split between the $1s \rightarrow \varphi^*_{LUMO+1}$ and $1s \rightarrow \varphi^*_{LUMO+2}$, which represents the difference between the two S atoms within each disulfide group. The difference between the constrained disulfide in the 5-membered ring of thioctic amide and the strain-free disulfide of cystine is also successfully reproduced in the 1.6 eV $1s \rightarrow \varphi^*_{LUMO+2}$, $1s \rightarrow \varphi^*_{LUMO+3}$ split that uniquely characterizes the former molecule.

4. Discussion

4.1. Contributions to sulfur K-edge XAS spectral shape

Sulfur K-edge X-ray absorption spectra principally consist of the dipole-allowed S 1s→np + continuum transitions. The nearly monotonic shift of sulfur K-edge transition energy with the formal sulfur valence state has until now been primarily attributed to changes in charge on the absorbing sulfur atom (Q^S_{mol}). These assignments were made in analogy with the systematic results produced by X-ray photoelectron spectroscopy (XPS) [50]. However the transition energies of sulfur XPS correspond to the sulfur 1s→continuum excitation (for sulfur 1s XPS), which provides a measure of the total energy of the atomic potential. In contrast, the energies of sulfur K-edge XAS are dominated by the difference in energy between S 1s and the np valence orbitals, which provide a measure of the core-to-valence energy difference *within* the atomic potential. Because the energy of the continuum is not affected by changes in Q^S_{mol}, XPS spectra dominantly reflect the systematically deeper energy of the sulfur core binding energies as Q^S_{mol} increases with oxidation state. However, as shown in two recent studies, an increase in Q^S_{mol} shifts all orbitals affected by the core potential to deeper binding energy [51,52]. Thus, both the valence orbitals and the core orbitals of sulfur shift to deeper binding energy by an almost equal amount as Q^S_{mol} increases. This leads to a smaller effect of Q^S_{mol} on the energies of sulfur K-edge XAS transitions than might be expected from an XPS perspective.

A computational comparison of **1a** and **1b** indicated that the core and valence orbitals are almost equally affected by the change in charge. However, the increase in bonding interaction represented by the change from two to three –Me ligands destabilizes the φ^*_{LUMO} to higher energy. It is this effect, not the increased charge, that dominates the shift in the sulfur K-edge transition energies. A comparison of the DFT calculated energy levels for $S(Me)_2$ and $[S(Me)_2]^{+\cdot}$ indicated that the $1s \rightarrow \varphi^*_{LUMO}$ transition would be at lower energy in $[S(Me)_2]^{+\cdot}$ even though the charge on sulfur increases relative to $S(Me)_2$. Similarly, in the case of **3a** and **3b**, the $1s \rightarrow \varphi^*_{LUMO}$ transition in **3b** occurs at lower energy even though the average Mulliken charge on **3b** (~0.020) is higher than **3a** (0.012). A comparison of the DFT generated sulfur K-edge spectra of **2a** and **2b**, and **3a** and **3b**, indicate that the extent of bonding and overlap of S with the carbon/oxygen atoms ultimately determines the intensity of the individual transitions. These examples indicate that bonding effects play a dominant role in determining the energy positions and intensities of sulfur K-edge transitions. It is typically the case, however, that bond strength increases with oxidation state. This is especially true for first and second row non-metals, with sulfur as a prime example. Low-valent sulfur rarely supports more than two bonds, while an increase in the number and dipolar character of sulfur–ligand bonds can be thought either to induce, or to follow from, the valence state of sulfur. For this reason, a systematic correlation may always be found between XAS rising-edge energy and the effective nuclear charge of the absorber. However, this correlation is not direct. Instead, it arises as a consequence of the systematics of the bonding changes that follow from oxidation state, rather than from oxidation state itself. That is, the shift in XAS rising-edge energy follows not from the Q^S_{mol} of the absorbing atom, but rather from the increased bonding and changes in valence orbital mixing that in turn follow from Q^S_{mol}.

4.2. Quantitation of sulfur speciation

Sulfur K-edge X-ray absorption spectra of three related sets of functional groups have been measured and the differences in their spectral shape explained using DFT calculations. The three functional pairs considered here are in three different oxidation states indicating that small changes in structure can dramatically affect the sulfur K-edge XAS spectra, and this effect is observed over all sulfur-containing species. Sulfur K-edge XAS has been applied to several systems to identify and quantify sulfur functionalities. In most cases, the unknown sulfur K-edge

spectrum is simulated with a proportional combination of sulfur K-edge spectra of relevant functional groups, and quantification of different sulfur functionalities is made based on the best simulation. Such analyses usually assume that changes in molecular structure have a negligible effect on the sulfur K-edge spectra of a given sulfur functional group, and a representative spectrum from some standard functional group can be used to fit the sulfur K-edge spectrum of an unknown species and to quantify that specific functional group.

In this study, it is shown that changes in molecular structure can lead to dramatic changes in the sulfur K-edge spectra of otherwise identical functional groups. Although identification of the oxidation state of an unknown sulfur species is feasible, true quantification of functional groups requires structurally accurate reference sulfur K-edge XAS spectra. For example, the sulfur K-edge spectrum of Na_2SO_4 cannot be used generically to simulate the SO_4^{2-} content of an unknown sample, or even of a transition metal sulfate [53]. To further emphasize this point, Fig. 8 compares the numerically-generated sulfur K-edge XAS of an equal mixture of cysteine, **2a**, **3a**, and aqueous inositol hexasulfate to that of methionine, **2b**, **3b**, and aqueous SO_4^{2-}. Both spectra have an equal mixture of RSR′ (R′ = H–, CH_3–), disulfide, organic sulfite, and ionic sulfate. However, the two spectral shapes differ significantly. At best, a qualitative estimate on the presence of certain functional groups can be made from the two spectra. This is further complicated by self-absorption, which can dampen the signal by decreasing the intensity and increasing the half width of spectral features. The sample spectra chosen to simulate an unknown sulfur K-edge spectrum should thus reflect the anticipated state of sulfur in the experimental sample so as to maximize the accurate speciation of quantified sulfur. In speciating a true unknown, it may be necessary to test several different forms of a given functional group, or even different particle sizes of a given

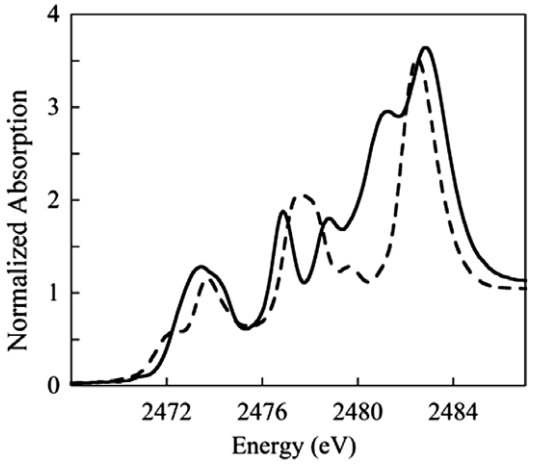

Fig. 8. Synthetic sulfur K-edge XAS spectra, consisting of a numerical admixture of 25% each of: (—), cysteine, cystine, ethylene cyclic sulfite, and *myo*-inositol hexasulfate, and; (----), methionine, (±)6-thioctic amide, dimethylsulfite, and sulfate. All except (±)6-thioctic amide were measured as solutions.

model [54], to obtain a truly relevant fit. In this way, the sensitivity to bonding of sulfur K-edge XAS spectra can be exploited to gain structural or aggregational information beyond the identification of functionality.

To summarize, the shift in sulfur K-edge XAS spectra previously thought to be due to oxidation state is instead dominated by the systematic changes in bonding that follow from increased oxidation state. Only minor contributions come from change in effective nuclear charge itself. Second, changes in the geometric structure around sulfur can strongly affect sulfur–ligand bonding and thus the mixing of atomic orbitals and the energies of molecular orbitals. This in turn can significantly change the sulfur K-edge spectra of otherwise identical sulfur functional groups. These results should be kept explicitly in mind when determining the speciation and quantities of sulfur in complex chemical, biological, or geological materials.

Acknowledgements

This publication was made possible by Grant Number 5 P41 RR001209 from the National Center for Research Resources (NCRR), a component of the National Institutes of Health (NIH). Its contents are solely the responsibility of the authors and do not necessarily represent the official view of NCRR or NIH. SSRL operations are funded by the Department of Energy, Office of Basic Energy Sciences. The SSRL Structural Molecular Biology program is supported by the National Institutes of Health, National Center for Research Resources, Biomedical Technology Program and by the Department of Energy, Office of Biological and Environmental Research. R.S thanks Prof. E.I. Solomon for an inspiring introduction to electronic structure calculations.

Appendix A. Supplementary material

Supplementary data associated with this article can be found, in the online version, at doi:10.1016/j.ica.2007.05.047.

References

[1] G.N. George, M.L. Gorbaty, J. Am. Chem. Soc. 111 (1989) 3182.
[2] G.N. George, M.L. Gorbaty, S.R. Kelemen, M. Sansone, Energy Fuels 5 (1991) 93.
[3] J.S. Waldo, O.C. Mullins, J.E. Penner-Hahn, S.P. Cramer, Fuel 71 (1992) 53.
[4] B. Akabayov, C.J. Doonan, I.J. Pickering, G.N. George, I. Sagi, J. Synchrotron Radiat. 12 (2005) 392.
[5] F. Jalilehvand, Chem. Soc. Rev. 35 (2006) 1256.
[6] G.P. Huffman, S. Mitra, F.E. Huggins, N. Shah, S. Vaidya, F. Lu, Energy Fuels 5 (1991) 574.
[7] G.P. Huffman, N. Shah, F.E. Huggins, L.M. Stock, K. Chatterjee, J.J. Kilbane II, M.-I.M. Chou, D.H. Buchanan, Fuel 74 (1995) 549.
[8] K. Sugawara, Y. Enda, T. Sugawara, M. Shirai, J. Synchrotron Radiat. 8 (2001) 955.
[9] D. Solomon, J. Lehmann, C.E. Martínez, Soil Sci. Soc. Am. J. 67 (2003) 1721.

[10] R. Wiltfong, S. Mitra-Kirtley, O.C. Mullins, B. Andrews, G. Fujisawa, J.W. Larsen, Energy Fuels 19 (2005) 1971.
[11] J. Prietzel, J. Thieme, M. Salomé, H. Knicker, Soil Biol. Biochem. 39 (2007) 877.
[12] O.B. Drury, S. Friedrich, S.J. George, S.P. Cramer, Nucl. Instr. Meth. Phys. Res. A 559 (2006) 728.
[13] P. Frank, B. Hedman, R.M.K. Carlson, K.O. Hodgson, Inorg. Chem. 33 (1994) 3794.
[14] I.J. Pickering, R.C. Prince, T. Divers, G.N. George, FEBS Lett. 441 (1998) 11.
[15] P. Frank, B. Hedman, K.O. Hodgson, Inorg. Chem. 38 (1999) 260.
[16] P. Frank, S. DeBeer George, E. Anxolabéhère-Mallart, B. Hedman, K.O. Hodgson, Inorg. Chem. 45 (2006) 9864.
[17] K. Rose, S.E. Shadle, T. Glaser, S. de Vries, A. Cherepanov, G.W. Canters, B. Hedman, K.O. Hodgson, E.I. Solomon, J. Am. Chem. Soc. 121 (1999) 2353.
[18] R.K. Szilagyi, B.S. Lim, T. Glaser, R.H. Holm, B. Hedman, K.O. Hodgson, E.I. Solomon, J. Am. Chem. Soc. 125 (2003) 9158.
[19] B. Hedman, P. Frank, J.E. Penner-Hahn, A.L. Roe, K.O. Hodgson, R.M.K. Carlson, G. Brown, J. Cerino, R. Hettel, T. Troxel, H. Winick, J. Yang, Nucl. Instr. Meth. A 246 (1986) 797.
[20] B. Hedman, P. Frank, S.F. Gheller, A.L. Roe, W.E. Newton, K.O. Hodgson, J. Am. Chem. Soc. 110 (1988) 3798.
[21] E. Anxolabéhère-Mallart, T. Glaser, P. Frank, G. Aliverti, J. Zanetti, B. Hedman, K.O. Hodgson, E.I. Solomon, J. Am. Chem. Soc. 123 (2001) 5444.
[22] G.N. George, EXAFSPAK & EDG_FIT. Stanford Synchrotron Radiation Laboratory, Stanford Linear Accelerator Center, Stanford University, Stanford, CA 94309, 2000.
[23] M.J. Frisch, G.W. Trucks, H.B. Schlegel, G.E. Scuseria, M.A. Robb, J.R. Cheeseman, J. Montgomery, J.A., T. Vreven, K.N. Kudin, J.C. Burant, J.M. Millam, S.S. Iyengar, J. Tomasi, V. Barone, B. Mennucci, M. Cossi, G. Scalmani, N. Rega, G.A. Petersson, H. Nakatsuji, M. Hada, M. Ehara, K. Toyota, R. Fukuda, J. Hasegawa, M. Ishida, T. Nakajima, Y. Honda, O. Kitao, H. Nakai, M. Klene, X. Li, J.E. Knox, H.P. Hratchian, J.B. Cross, V. Bakken, C. Adamo, J. Jaramillo, R. Gomperts, R.E. Stratmann, O. Yazyev, A.J. Austin, R. Cammi, C. Pomelli, J.W. Ochterski, P.Y. Ayala, K. Morokuma, G.A. Voth, P. Salvador, J.J. Dannenberg, V.G. Zakrzewski, S. Dapprich, A.D. Daniels, M.C. Strain, O. Farkas, D.K. Malick, A.D. Rabuck, K. Raghavachari, J.B. Foresman, J.V. Ortiz, Q. Cui, A.G. Baboul, S. Clifford, J. Cioslowski, B.B. Stefanov, G. Liu, A. Liashenko, P. Piskorz, I. Komaromi, R.L. Martin, D.J. Fox, T. Keith, M.A. Al-Laham, C.Y. Peng, A. Nanayakkara, M. Challacombe, P.M.W. Gill, B. Johnson, W. Chen, M.W. Wong, C. Gonzalez, J.A. Pople. GAUSSIAN 03, Revision C.02, 2004.
[24] A.D. Becke, Phys. Rev. A 38 (1988) 3098.
[25] A.D. Becke, J. Chem. Phys. 98 (1993) 5648.
[26] J.P. Perdew, Phys. Rev. B 33 (1986) 8822.
[27] J.P. Perdew, K. Burke, Y. Wang, Phys. Rev. B 57 (1998) 14999.
[28] S.H. Vosko, L. Wilk, M. Nusair, Can. J. Phys. 58 (1980) 1200.
[29] P.C. Hariharan, J.A. Pople, Theor. Chim. Acta 28 (1973) 213.
[30] M.M. Francl, W.J. Hehre, J.S. Binkley, M.S. Gordon, D.J. DeFrees, J.A. Pople, J. Chem. Phys. 77 (1982) 3645.
[31] V.A. Rassolov, J.A. Pople, M.A. Ratner, T.L. Windus, J. Chem. Phys. 109 (1998) 1223.
[32] J.E. Carpenter, F. Weinhold, THEOCHEM 169 (1988) 41.
[33] J.P. Foster, F. Weinhold, J. Am. Chem. Soc. 102 (1980) 7211.
[34] A.E. Reed, L.A. Curtiss, F. Weinhold, Chem. Rev. 88 (1988) 899.
[35] G. Schaftenaar, J.H. Noordik, Comput-Aided Mol. Des. 14 (2000) 123.
[36] A. Tenderholt, PYMOLYZE, Stanford University, Stanford, CA-94305, 2005.
[37] F. Neese, G. Olbrich, Chem. Phys. Lett. 362 (2002) 170.
[38] F. Neese. ORCA – An Ab-initio, DFT and Semiempirical Electronic Structure Package, Max-Planck Institut für Bioanorganische Chemie, Mülheim, Germany, November, 2004, Version 2.4, Revision 16, 2004.
[39] M. Alagar, R.V. Krishnakumar, A. Mostad, S.S. Natarajan, Acta Crystallogr., Sect. E 61 (2005) o1165.
[40] M. Jannin, R. Puget, C. de Brauer, R. Perret, Acta Crystallogr., Sect. C 47 (1991) 982.
[41] S. Dahaoui, V. Pichon-Pesme, J.A.K. Howard, C. Lecomte, J. Phys. Chem. A 103 (1999) 6240.
[42] R.M. Stroud, C.H. Carlisle, Acta Crystallogr., Sect. B 28 (1972) 304.
[43] R.M. Ibberson, M.T.F. Tellinga, S. Parsons, Acta Crystallogr., Sect. B 62 (2006) 280.
[44] F.P. Boer, J.J. Flynn, E.T. Kaiser, O.R. Zaborsky, D.A. Tomalia, A.E. Young, Y.C. Toag, J. Am. Chem. Soc. 90 (1968) 2970.
[45] G. Lowe, G.R.J. Thatcher, J.C.G. Turner, A. Waller, D.J. Watkin, J. Am. Chem. Soc. 110 (1988) 8512.
[46] S. DeBeer George, M. Metz, R.K. Szilagyi, H.X. Wang, S.P. Cramer, Y. Lu, W.B. Tolman, B. Hedman, K.O. Hodgson, E.I. Solomon, J. Am. Chem. Soc. 123 (2001) 5757.
[47] P. Frank, B. Hedman, R.M.K. Carlson, T.A. Tyson, A.L. Roe, K.O. Hodgson, Biochemistry 26 (1987) 4975.
[48] S. Mitra-Kirtley, O.C. Mullins, C.Y. Ralston, D. Sellis, C. Pareis, Appl. Spectrosc. 52 (1998) 1522.
[49] G. Sarret, J. Connan, M. Kasrai, G.M. Bancroft, A. Charrie-Duhaut, S. Lemoine, P. Adam, P. Albrecht, L. Eybert-Berard, Geochim. Cosmochim. Acta 63 (1999) 3767.
[50] A. Fahlman, K. Hamrin, J. Hedman, R. Nordberg, C. Nordling, K. Siegbahn, Nature (London) 210 (1966) 4.
[51] R. Sarangi, N. Aboelella, K. Fujisawa, W.B. Tolman, B. Hedman, K.O. Hodgson, E.I. Solomon, J. Am. Chem. Soc. 128 (2006) 8286.
[52] R. Sarangi, S. DeBeer George, D.J. Rudd, R.K. Szilagyi, X. Ribas, C. Rovira, M. Almeida, K.O. Hodgson, B. Hedman, E.I. Solomon, J. Am. Chem. Soc. 129 (2007) 2316.
[53] R. Szilagyi, P. Frank, S. DeBeer George, B. Hedman, K.O. Hodgson, Inorg. Chem. 43 (2004) 8318.
[54] I.J. Pickering, G.N. George, E.Y. Yu, D.C. Brune, C. Tuschak, J. Overmann, J.T. Beatty, R.C. Prince, Biochemistry 40 (2001) 8138.